The Effects of Electron Cyclotron Absorption in Powerful Narrow-Band sub-THz Oscillators Exploiting Volume and Surface Modes

A. J. MacLachlan, C. W. Robertson, A. W. Cross, *Member, IEEE* and A. D. R. Phelps, *Member, IEEE*

***Abstract*— We present the theory, design and numerical modeling of novel, pulsed sub-THz oscillators based on cylindrical, two-dimensional (2D) periodic surface lattice (PSL) interaction cavities. Investigation of the electronic efficiency and power dependence on the magnitude of the magnetic guide field and the electron beam current is investigated. While cyclotron absorption effects have been studied in low order, 1D BWOs, few studies have considered cyclotron absorption in highly overmoded, 2D-PSL oscillators. Here we investigate certain behavior associated with cyclotron absorption in 2D-PSL devices with over 400 modes. This electron cyclotron absorption is shown to be a universal process, independent of frequency and transverse cavity size. Dispersive behavior shows minimal group velocity at the point of interaction and demonstrates similarities with degenerate band edge phenomena. In this work, the fundamental mode selection mechanism relies on the coupling of high-order volume and surface waves. Good agreement between theory and modeling is presented.**

***Index Terms*— Cherenkov, electron beam, mm-wave, mode coupling, periodic structure, cyclotron absorption, radiation source, terahertz.**

I. Introduction

Vacuum electronic devices have significantly evolved since they were first conceived one century ago. Renewed interest in vacuum electronics has been stimulated by contemporary advances in materials and composite materials technology, metamaterials, nanofabrication and electromagnetic (EM) simulation tools; establishing new frontiers in the development of powerful sources at sub-THz and THz frequencies. One type of vacuum electronic device that shows promise for the realization of intense, high frequency, pulsed sources, is an oscillator based on an intricate, two-dimensional surface structure [1-11].

We present the design of slow-wave oscillators, based on metal cylindrical, two-dimensional (2D) periodic surface lattice (PSL) interaction cavities (with EM properties similar to those of a cylindrical waveguide lined with a dielectric material [1,11,30,31]). Achieving high output peak power while simultaneously bridging the 'THz-gap' requires the use of an 'oversized' interaction cavity in which the diameter, D is several times the operating wavelength, λ. Complex boundary conditions imposed by the 2D-PSL on the inner cavity wall restrict the number of modes within the oversized system, facilitating single-frequency output. Vital heat dissipation and thermal regulation are enabled by the metallic wall of the cavity on which the sinusoidal corrugation is machined. The 2D corrugation provides the additional benefit of mitigating charge accumulation and RF breakdown. Employing 2D geometry (in place of the 1D corrugation typically favored in conventional surface wave and backward wave oscillators (BWOs) [12-16]) can enhance the spectral purity, output power and electronic efficiency of the device [11]. Diverse, high-impact applications of the pulsed 2D-PSL sources include: communications, environmental sensing, dust cloud monitoring, enhancing nuclear magnetic resonance (NMR) spectroscopy using dynamic nuclear polarization (DNP-NMR), long range imaging, pulsed high-frequency electron paramagnetic resonance (EPR) for biomolecular characterization, non-destructive testing, plasma scattering diagnostics and radar systems [17-24].

The 2D-PSL mode selection mechanism involves the coupling of 'partial' volume and surface waves. Such resonant coupling is possible when the Bragg resonance conditions are satisfied. The azimuthal Bragg condition is: $\bar{m} = m_v + m_s$ (where $\bar{m}$ is the number of azimuthal variations around the circumference of the cylinder and $m_{v,s}$ is the number of azimuthal variations of the volume v and surface s waves), while the longitudinal Bragg condition is expressed: $\bar{k} = \bar{k}_s - \bar{k}_v$ (where $\bar{k}_{v,s}$ is the wavevector of the volume v and surface s waves). Analytical dispersions illustrate four eigenwaves (with approximately equal wavenumbers); similar to the four-eigenmode super-synchronization discussed in [27]. However, in this work, the 2D-PSL dispersion is comprised of volume and surface waves and the degeneracy condition [25-28] was not considered.

This paper builds on the concepts developed in [11], delving further into the 2D-PSL behavior;in particular, the effects of electron cyclotron absorption. Although these effects have been well researched in 1D BWOs, no explicit studies have been made of cyclotron absorption in 2D oscillators. In this paper, we demonstrate electron cyclotron absorption in 2D-PSL oscillators at two different frequencies, based on cavites with different diameter-to-wavelength ratios, D/λ. Analytical and numerical results show the electron cyclotron absorption resonance at 176GHz (D/λ~5.5) and 351GHz (D/λ~3.5). The parameters of the 176GHz 2D-PSL are: axial period, $d_z = 2\pi/\bar{k}_z$ =0.78mm (where $\bar{k}_z$ is the lattice wavevector); corrugation amplitude Δr=0.25mm; mean radius r_0 = 4.5mm and $\bar{m}$ =16 azimuthal variations. The design of the D/λ~3.5, 351-GHz oscillator (r_0 =1.47mm; $\bar{m}$ =10; d_z =0.39mm) is discussed in [11]. For optimum performance and efficiency,

This work has been supported by the Air Force Office of Scientific Research (AFOSR), award numbers FA8655-13-1-2132 and FA9550-17-1-0095. A. J. MacLachlan, C. W. Robertson, A. W. Cross and A. D. R. Phelps are with the Department of Physics, SUPA, University of Strathclyde, Glasgow, G4 0NG UK
(e- mail: amy.maclachlan@strath.ac.uk, craig.robertson@strath.ac.uk, a.w.cross@strath.ac.uk and a.d.r.phelps@strath.ac.uk).

magnetic fields in the region of this cyclotron resonance are best avoided, and the results presented in this paper are important for future designs at different frequencies. The 2D-PSL cavities can be fabricated using copper electrodeposition [1,4] or additive manufacturing [6].

II. Theory

The EM field inside a cylindrical 2D-PSL can be derived by considering a smooth cylindrical waveguide (of finite length) with a fictious magnetic surface current, $\boldsymbol{j}_m$. The sinusoidal 2D periodic corrugation, p

$$p = r_0 + \Delta r cos(\bar{m}\varphi)\cos(\bar{k}_z z) \tag{1}$$

can be described in terms of an equivalent magnetic surface current by imposing the following boundary condition:

$$\boldsymbol{j}_m = \boldsymbol{n} \times [\boldsymbol{\nabla}(p\boldsymbol{E} \cdot \boldsymbol{n})] + i\omega p \boldsymbol{n} \times [\boldsymbol{n} \times \boldsymbol{H}] \tag{2}$$

The bold font indicates quantities with 3-vectors, i.e. the electric $\boldsymbol{E}$ and magnetic $\boldsymbol{H}$ field and normal unit vector, $\boldsymbol{n}$**.** The transverse electric and magnetic fields are expanded from Maxwell's curl equations and described as wave packets with slowly varying amplitudes ($C_q^{e,h}$) filled with fast oscillating terms. The electric and magnetic fields are described as a summation of the complete set of eigenmodes, q as described in [4, 30, 31]. For the stationary regime, where localized surface fields are coupled to the non-propagating (near cut-off) azimuthally symmetric $TM_{0,N}$ volume mode, the power transmitted through the cylinder is defined by integrating the Poynting vector over the cylindrical cross section to obtain the wave equation:

$$\nabla_z^2 C_q^{v,s}(z) + \omega\delta C_q^{v,s}(z) \mp \frac{\bar{\omega}\Delta}{c^2} C_q^{v,s}(z) = N_{v,s} \oint \boldsymbol{j}_m . \boldsymbol{H}_{q'}^* \, d\sigma \tag{3}$$

Here, $C_q^{v,s}$ is the slowly varying amplitude of the magnetic field of the 'partial' volume and surface fields, δ is the Bragg detuning (which can be complex with the imaginary component describing losses) and $\bar{\omega}$ is the mean frequency of the volume and surface fields. The wave norm $N_{v,s}$ for the volume $(-)$ and surface fields $(+)$ is $N_{v,s} = i\omega\varepsilon_0 / \oint \boldsymbol{H}_q . \boldsymbol{H}_{q'}^* \, d\sigma$, where $\boldsymbol{H}_{q'}^*$ is the complex conjugate of the magnetic field of the eigenmode [4, 29, 31]. Eq.(2) is substituted into the left hand side of Eq.(3) which (for volume and surface wave coupling) must be non-zero. Averaging over the fast oscillation terms and renormalizing as outlined in [3, 29, 31] gives the coupled 2D-PSL dispersion relation:

$$(\omega_e^2 - \Lambda^2)\{\Lambda^4 - 2\Lambda^2[(2 + \Gamma^2 + \omega_e^2) + (2 - \Gamma^2 + \omega_e^2)^2]\} = 2\alpha^4(2 - \Gamma^2 + \omega_e^2 - \Lambda^2) \tag{4}$$

where Λ is the normalized wave vector, ω_e is a variable angular frequency, $\Gamma = c\bar{k}_z/\Delta\omega$ is a geometrical detuning parameter where $\Delta\omega = \sqrt{(\omega_c^v)^2 + (\omega_c^s)^2/2}$ and $\omega_c^{v,s}$ is the angular cut-off frequency of the volume and surface modes and α is the normalized coupling coefficient (which determines the strength of the coupling of the volume and surface fields). The dispersive EM properties of the structure can be predicted by evaluating the normalized coupling coefficient, α:

$$\alpha = \frac{\pi\omega^2\varepsilon_0 r_0 \Delta r \beta}{2}$$

where ε_0 is the permittivity of free space and β is written:

$$\beta = \sqrt{\frac{\left(H_{q,\tau}^{*,v} \cdot H_{q,\tau}^{s}\right)\left(H_{q,\tau}^{*,s} \cdot H_{q,\tau}^{v}\right)}{\oint\left(H_q^{*,v} \cdot H_{q'}^{v}\right)d\sigma \oint\left(H_q^{*,s} \cdot H_{q'}^{s}\right)d\sigma}}$$

The strength of the coupling can also be estimated by comparing analytical studies with numerical Particle-in-Cell (PiC) calculations.

III. Dispersion Analysis

Previous studies have revealed that the geometrical detuning parameter Γ can define the operating regime of the system, i.e. determining whether a backward wave, or a pi-point or a forward wave interaction takes place. Within a certain parameter space ($\Gamma \sim 1.8 - 2.1$, $\alpha \sim 0.4 - 0.9$), a 'flat' [11,30] dispersion curve can be observed. Analytical dispersion diagrams (obtained by solving Eq.4 [4,11,29,31]) in Fig.1 depict the interaction between the 2D-PSL eigenmode and a modulated, 100kV electron beam (solid black line): $\omega = k_z v_z + (\bar{k}_z v_z)$. The inclusion of the $\bar{k}_z v_z$ term is valid for all slow wave devices in which the electron beam passes close to a periodic cavity. The normalized dispersion in Fig.1(a) is composed of three distinct branches. The lowest branch (formed primarily from the 'partial' $TM_{0,6}$ volume mode) exhibits a relatively flat profile and a correspondingly slow group velocity. Normalized numerical data (dot-dash red), obtained by modeling the periodic unit cell of the 2D-PSL using the CST Eigenmode Solver, shows good general agreement with the lower analytical dispersion branch when $k_z/\bar{k}_z \sim -0.3,..,0.3$. Deviations beyond this region can be attributed to key differences between the two models; namely the inclusion of spatial harmonics in the CST Eigenmode Solver. The theoretical results are calculated by taking into account just one spatial harmonic of the coupled eigenmode, though in practice, coupling between these spatial harmonics can be assumed. The dashed gray lines indicate additional valid eigenwave solutions to Eq.(4). These eigenwaves, together with the annotated forward and backward propagating waves, demonstrate the existence of four degenerate eigenwaves at ~176-GHz; $k_z/\bar{k}_z \sim 0.46$ (dotted grey line). These findings have relevance to the work on four-eigenmode super-synchronization [25-28] where a degenerate band edge (DBE) has been shown to provide mode selection in a range of vacuum electronic (as well as optical) devices. However, unlike a DBE mode, the flattened dispersion curve of the 2D-PSL oscillator is formed by the intersection of the 'partial' $TM_{0,6}$ volume (dashed yellow curve) and 'partial' surface (dashed green curve) fields as shown in Fig.2(b). The imaginary solutions are indicated by the dotted black line, and the red circle marks the interaction between the coupled 2D-PSL eigenfield and the 100kV electron beam.

Simulations indicate that a similar, albeit lower efficiency, result can be obtained in the positive k_z region using a lower voltage electron beam. However, since the aim is to achieve a backward Cherenkov (absolute) instability, the group velocity should be negative.

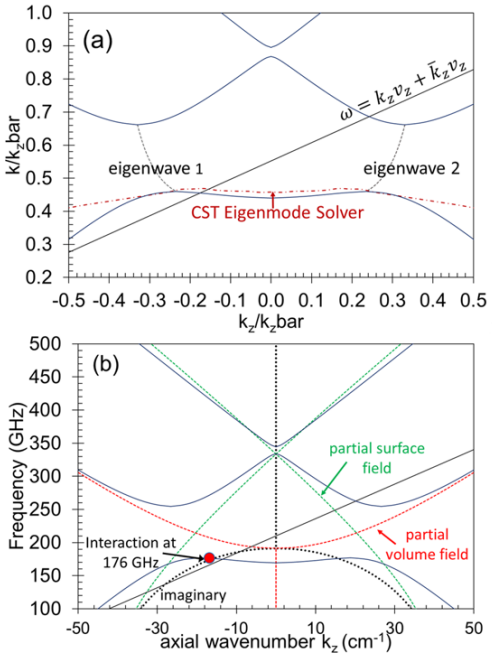

Fig.1. Analytical dispersion diagrams for $D/\lambda = 5.5$, 176-GHz, 2D-PSL (a) Normalized dispersion plot comparing analytical solutions to the CST Eigenmode solver (dot-dash-red) result. (b) Dispersion plot showing interaction between coupled eigenmode (solid-blue) and 100kV modulated electron beam at 176-GHz. The partial volume (dashed red), partial surface (dashed green) and imaginary (dotted-black) solutions are shown.[37]

IV. Numerical PiC Model

The numerical PiC model of the $D/\lambda = 5.5$, 176-GHz, 2D-PSL oscillator has been created using CST Particle Studio (CST-PS). A detailed description and diagrammatic representation of the general model is provided in [11]. The 2D-PSL interaction cavity (constructed from lossy copper walls with conductivity, $\sigma = 5.8 \times 10^7$ S/m), consists of n=12 complete axial periods with additional tapered periods at the input and output. The magnitude of the axial magnetic field is gradually tapered to zero such that the electrons, having passed through the 2D-PSL structure, are guided out to the wall in the smooth collector region of increased radius (4.95 mm), allowing the eigenmode to propagate from the structure. A thin (0.1mm) annular beam is launched from a planar emission site and accelerated directly towards a tungsten grid from a magnetic field immersed cathode. The accelerating electric field between the cathode and the grid is supplied via a discrete voltage port. The separation between the outer radius of the annular electron beam and the inner radius of the 2D corrugation is 0.02mm, enabling the beam to intercept the localized surface field. Designing a suitable electron gun to be deployed within a working prototype will involve further research. However, one type of cathode that can potentially supply the required high current densities with spatial and temporal control and fast turn-on capability, is a field emission array cathode [32].

V. Simulation Results

The backward Cherenkov interaction is driven by an axially injected electron beam with minimal perpendicular velocity. Unlike slow-wave electron cyclotron masers, which can also operate in the Cherenkov regime, no transverse interaction takes place (except in the case of cyclotron absorption where the $v_\perp/v_\parallel$ ratio can increase as the electron beam propagates through the 2D-PSL structure). The left-hand axis of Fig.2(a) shows the axial (black) and transverse (v_x, v_y; yellow, gray) electron beam velocities as a function of axial position at a time, 12ns. The right-hand axis (Fig.2(b)) illustrates the modulated electron energy (red) for an interaction between the pulsed electron beam (100kV,150A) and the 176GHz, D/λ~5.5 (Δr=0.25mm, r_0 = 4.5mm, $\bar{m}$ =16, d_z =0.78mm) 2D-PSL. The 3-dimensional electron energy trajectory in Fig.2(b) shows the azimuthal variation in electron energy imposed by the azimuthal corrugation.

Fig.3 shows the main spectral peak at 176-GHz and confirms that the power in the spatial harmonic at 352-GHz is acceptably low. The frequency of this generated radiation matches the interaction frequency predicted by the analytical dispersion in Fig.1(b). Contour plots illustrating the axial magnetic (left) and electric (right) field components of the $HE_{16,1}$ eigenmode (composed of the "partial" $TM_{0,6}$ volume field and the hybrid surface field) are presented in Fig.4. As observed from the $HE_{16,1}$ time domain signal in Fig.3(b), the majority (~2.2MW) of the total (~2.7MW) output power (corresponding to ~18% electronic efficiency) is in the $HE_{16,1}$ eigenmode, while the remaining power is contributed by the sum of the azimuthally symmetric $TM_{0,N}$ modes (N=1..6). The simulated efficiency is lower than that achieved in [11] due to the increased complexity of this more overmoded system, which might benefit from further optimization. Nevertheless, the fundamental proof-of-principle, high-order mode coupling and single-frequency excitation has been established, and the the coupling coefficient α~0.65 has been estimated by comparing the theoretical and simulation results.

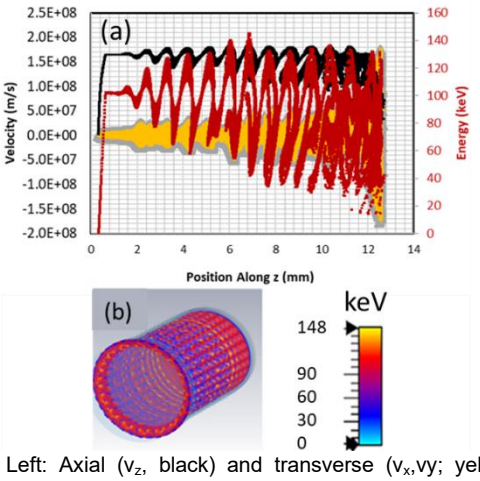

Fig.2. (a) Left: Axial (v_z, black) and transverse (v_x,v_y; yellow,gray) electron velocities [37]. Right: Electron energy (keV) at time, 12 ns, as a function of axial position (b) 3D visualization of electron energy, in keV.

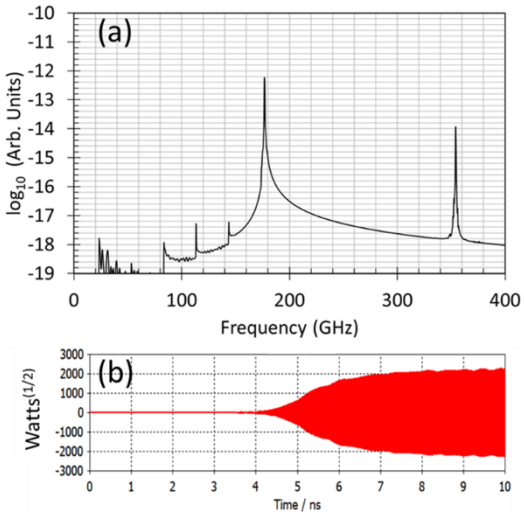

Fig.3. (a) CST-PS spectral peak at 176-GHz (dB scale) observed for the 2D-PSL with r_0 = 4.5mm, $\bar{m}$ =16, Δr=0.25mm, d_z =0.78mm [37]. (b) time domain signal for the $HE_{16,1}$ eigenmode with 2.2MW peak pulsed power.

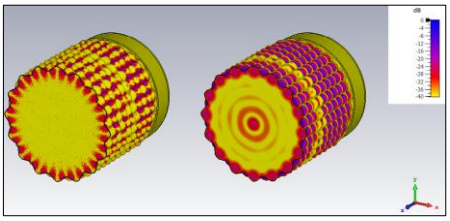

Fig.4. CST-PS axial magnetic (left) and electric (right) field contour plots

The dependence of the pulsed power and efficiency on the peak current (in the range I=10-100A) was investigated for the less overmoded, 351GHz device in [11]. This study has been extended to consider the power and efficiency as the current is incrementally increased up to I=400A. Simulation results for the D/λ = 3.5, 351-GHz (triangular marker) and D/λ = 5.5, 176-GHz (circular marker) devices are plotted in Fig.5. The input voltage V_0 was adjusted to compensate for the impedance of the discrete voltage port, thus maintaining the same effective voltage V_{eff} at very high peak currents, I >250A. Signficant detuning from the optimum interaction conditions, manifesting in reduced spectral purity and diminished power and efficiency, was otherwise observed. The black curves (Fig.5) represent the normalized electronic efficiency (calculated using V_{eff}) for the D/λ = 3.5, 351-GHz (triangular marker) and D/λ = 5.5, 176-GHz (circular marker) devices. The corresponding red and blue dotted lines indicate the overall device efficiency (calculated using V_0).

Results plotted in red (351-GHz) and blue (176-GHz) show the output pulsed power as a function of current. Simulations indicate that even the smaller (r_0 =1.47mm) cavity can accept 400A of pulsed current (peak current density, ρ~60Amm^{-2}) generating 6.6 MW of peak output power. In this case, the frequency spectrum is less clean, resulting in a broader bandwidth (~3 GHz). The spectral purity is retained at 400A for the larger radius (ρ~6.35Amm^{-2}) cavity. These results demonstrate the potential for extremely powerful, short pulse 2D-PSL oscillators with the principles of operation being applicable over a wide range of frequencies.

It is evident from Fig.5 that the 2D-PSL devices operate in different regimes below a threshold current (I_1~130A, f_1 =176-GHz; I_2,~60A,f_2 =351-GHz) and that launching a current close to these values is detrimental to the efficient operation of the device.

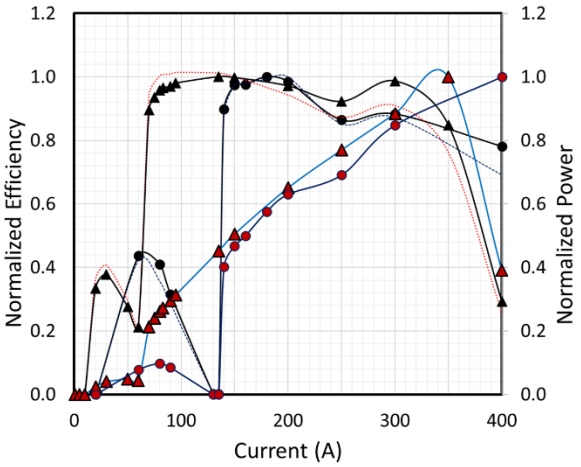

Fig.5. Left-hand axis: dependence of the electronic (solid black) and device (dotted) efficiency on electron beam current for the D/λ = 3.5, 351-GHz (triangular markers) and D/λ =5.5,176-GHz (circular markers) 2D-PSL devices. Right-hand axis: power as a function of current for the D/λ = 3.5, 351-GHz (red curve) and D/λ =5.5,176-GHz (blue curve) 2D-PSL devices.

Having established, both theoretically and numerically, that the D/λ=5.5, 176-GHz oscillator operates in a similar manner to the D/λ=3.5, 351-GHz device discussed in [11], the effects of cyclotron absorption in both oscillators can be studied and compared. Fig.6 illustrates the efficiency dependence on the magnitude of the magnetic guide field, plotted from the CST-PS simulation results for the D/λ=3.5, 351-GHz (triangular markers) and D/λ=5.5 176-GHz (circular markers) 2D-PSL oscillators. For weak B- fields (< 2T) electrons were collected on the wall due to inadequate beam transport. The results demonstrate peak efficiency at ~3T at both 176-GHz and 351-GHz. While, in conventional BWOs, peak efficiency is generally observed at higher B-fields, above the cyclotron absorption region, 1D BWOs that perform efficiently with modest guide fields have been reported [33]. In BWO devices, the magnetic guide field transports electrons with minimal perpendicular velocity, $v_\perp$. However, near the cyclotron resonance, where fast (FCM) or slow (SCM) cyclotron beam modes couple with the eigenmode of the interaction cavity, electrons typically deviate from their axial trajectory. In Fig.6, the prominent dips at ~8.00-8.75T and ~14.50-16.00T are suggestive of cyclotron absorption. Although cyclotron absorption in conventional Cherenkov oscillators has been well-researched [34-36], few studies have hitherto been carried out for 2D-PSL devices. The relativistic electron cyclotron frequency is defined:

$$f_{ce} = \frac{eB}{2\pi\gamma m_e} \tag{5}$$

where e is the electronic charge, B is the magnitude of the magnetic guide field, m_e is the electron mass, γ is the

relativistic Lorentz factor, $\gamma \sim 1 + V/511$ and V is the electron beam voltage in kV. From Eq.5, the cyclotron wave frequency f_{ce} matches the frequency of the generated wave when B=7.50T and B=14.73T (for the 176-GHz and 351-GHz 2D-PSLs respectively). However, the cyclotron absorption effect is more accurately determined by the location of the intersection of the cyclotron beam mode with the 2D-PSL "cold" dispersion curve and is further complicated by the periodicity of the dispersion relation. From Floquet's Theorem, the spatial harmonics of the 2D-PSL dispersion curves are separated along k_z by $\bar{k}_z$, giving an infinite number of FCMs and SCMs. The relativistic electron cyclotron frequency hence provides only an approximation to where the electron cyclotron resonance absorption will occur.

More accurate theoretical predictions for the (a) 176-GHz and (b) 351-GHz devices are shown in Fig.7. In Fig.7(a.b) the SCM of the $l = 2$ electron beam, $\omega_{ce} = k_z v_z + l(\bar{k}_z v_z) - \tilde{n}(\Omega_{ce})$ with angular electron cyclotron frequency, Ω_{ce} interacts with the 2D-PSL eigenmode in the first Brillouin zone ($-0.5 < k_z/k_{ce} < 0.5$). The dotted green line shows the f_{ce}~188GHz, $\tilde{n} = 1$ (B=8.00T) SCM intersecting the 2D-PSL eigenmode near the pi-point at 177-GHz. The dot-dash green line (B=8.75T, f_{ce}~206-GHz, $\tilde{n} = 1$ SCM) shows a backward wave interaction with the eigenmode at 175GHz.

The $\tilde{n} = 1$ SCM of the synchronous ($l = 1$) electron beam (B=8.00T, f_{ce}~188GHz, dotted red) intersects the second spatial harmonic of the 2D-PSL eigenmode harmonic in the second ($0.5 < k_z/k_{ce} < 1.5$) Brillouin zone (while the f_{ce}~206-GHz (B=8.75T) SCM crosses the second and third Brillouin zones. An interaction between the $\tilde{n} = 1$, FCM and the -1 spatial harmonic of the 2D-PSL eigenmode is also possible. Fig.7(b) shows the $l = 2$, $\tilde{n} = 1$, f_{ce}~377-GHz (B=16.00T) SCM intersecting the 351-GHz 2D-PSL eigenmode at ~344-GHz. Overall, Fig.7 confirms that the efficiency minima observed in Fig.6 correspond to cyclotron absorption. Disadvantages in designing a device where the magnitude of the axial magnetic field is within the region of the electron cyclotron frequency are twofold: greatly diminished, and often negligible, output power and efficiency; and an increase in electron energy spread. For this reason, these axial magnetic field magnitudes are best avoided, and a suitable axial magnetic field (on either side of the cyclotron resonance) should therefore be chosen.

Fig.6 illustrates that the separation between the maxima and minima ($\Delta B_{1,2}$) scales with the operating frequency; i.e. $\Delta B_1/\Delta B_2 \sim f_1/f_2$ (where $f_{1,2} = 176$; 351GHz). Based on these findings, W-band (75-110 GHz), ~ 100kV 2D-PSL oscillators (for which cyclotron absorption is predicted to occur around ~3.2T at the lower end of the spectrum) may operate less efficiently at ~3T. While this can potentially be resolved by increasing the voltage and scaling d_z accordingly, simulating these 2D-PSL devices at higher magnetic fields could nevertheless provide a more realistic starting point when exploring initial design parameters.

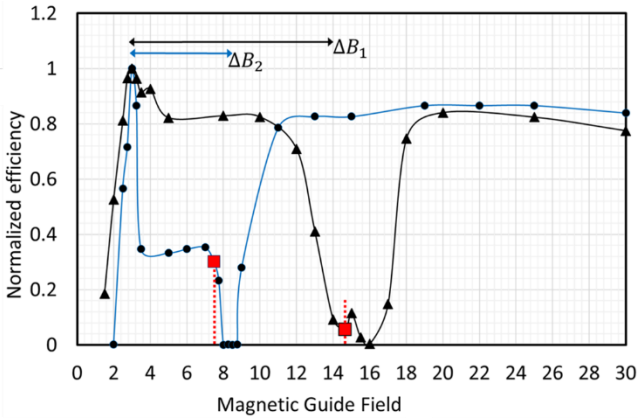

Fig.6. Normalized efficiency dependence on the magnitude of the magnetic guide field for the 351 GHz (triangular marker) and 176 GHz (circular marker) 2D-PSL devices. The red squares indicate the magnetic field values of 7.5T and 14.7T, for which the relativistic cyclotron frequency (calculated from Eq. 5) equals 176 GHz and 351 GHz respectively.

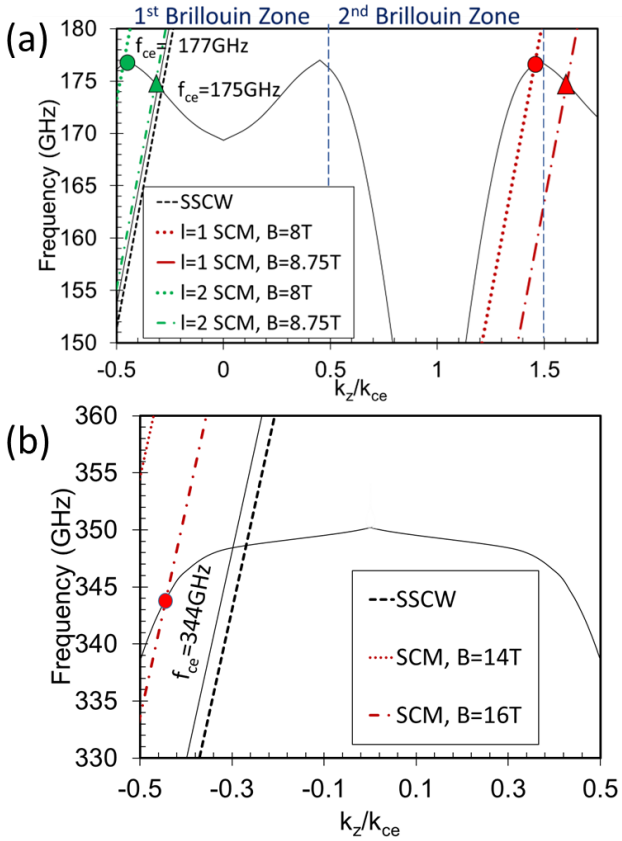

Fig.7(a) Interaction of slow cyclotron modes with f_{ce}=188, 206GHz (corresponding to B=8.00, 8.75T) with the eigenmode of the 176-GHz 2D-PSL in the first, second (and start of the third) Brillouin zones. b) Interaction of electron cyclotron modes with f_{ce}=330, 377GHz (corresponding to B=14, 16T) with the eigenmode of the 351-GHz 2D-PSL in the first Brillouin zone.

VI. Conclusion

Theoretical and numerical studies of electron cyclotron absorption in highly overmoded oscillators based on 2D-PSL interaction structures have been carried out at two different frequencies; 176GHz and 351GHz. The cyclotron absorption dip manifests within a narrow axial magnetic field range,

which is shown to scale directly with frequency. This universal observation is independent of the diameter-to-wavelength ratio of the cavity. An interesting feature of these devices is the potential for efficient operation at modest axial magnetic field magnitudes of around 3T.

Few studies of electron cyclotron absorption in sources based on highly overmoded 2D interaction cavities have hitherto been made. This work demonstrates the importance of choosing an appropriate magnetic field, sufficiently far from the electron cyclotron resonance. When suitable magnetic field magnitudes are chosen, simulations of the overmoded 176-GHz and 351-GHz 2D-PSL oscillators exhibit megawatts of output power. Excellent spectral purity is observed when the geometrical cavity dimensions and electron beam parameters are correctly chosen according to the analytical theory. The current of the electron beam has been shown to affect not only the electronic efficiency of the wave-beam interaction, but also the operating regime of the device. Overall, good agreement between the CST particle-in-cell simulations and the analytical theory has been demonstrated. These results are applicable to future designs of 2D-PSL oscillators at different frequencies.

ACKNOWLEDGMENT

We would like to commemorate our dear friend and colleague, Prof. Adrian W. Cross, the leader of the Atoms, Beams and Plasmas group at the University of Strathclyde, who sadly and unexpectedly passed away on 21st January 2023. His presence and scientific contributions will be greatly missed.

Useful discussions with Dr. Ivan Konoplev of the UK Atomic Energy Authority are gratefully acknowledged.

REFERENCES

[1] I. V. Konoplev, A. J. MacLachlan, C. W. Robertson, A. W. Cross and A. D. R. Phelps, "Cylindrical periodic surface lattice as a metadielectric: concept of a surface-field Cherenkov source of coherent radiation", *Phys. Rev. A*, vol. 84, no. 013826, July 2011, doi: 10.1103/PhysRevA.84.013826

[2] N. S. Ginzburg, A. M. Malkin, A. S. Sergeev, and V. Y. Zaslavsky, "Quasi-optical theory of relativistic submillimeter surface-wave oscillator," *Appl. Phys. Lett*., vol. 99, no. 121505, Sept. 2011, doi:10.1063/1.3641868

[3] N. S. Ginzburg, A. M. Malkin, A. S. Sergeev, and V. Y. Zaslavsky, "Powerful surface-wave oscillators with two-dimensional periodic structures," *Appl. Phys. Lett*., vol. 100, no. 143510, Mar. 2012, doi: 10.1063/1.3701580

[4] I. V. Konoplev, A. J. MacLachlan, C. W. Robertson, A. W. Cross and A. D. R. Phelps, "Cylindrical, periodic surface lattice – theory, dispersion analysis and experiment", *Appl. Phys. Lett*., vol. 101, no. 121111, Sept. 2012, doi:10.1063/1.4754572

[5] N. S. Ginzburg, A. M. Malkin, I. V. Zheleznov and A. S. Sergeev, "Evanescent waves propagation along a periodically corrugated surface and their amplification by relativistic electron beam (quasi-optical theory)", *Phys. Plasmas*, vol. 20, no. 063105, June 2013, doi: 10.1063/1.4811388

[6] A. R. Phipps, A. J. MacLachlan, C. W. Robertson, L. Zhang et al., "Electron beam excitation of coherent sub-terahertz radiation in periodic structures manufactured by 3D printing", *Nucl. Instrum. Methods Phys. Res. Sect. B*, vol. 402, pp. 202-205, July 2017, doi: 10.1016/j.nimb.2017.03.093

[7] N. S. Ginzburg, E. V. Ilyakov, I. S. Kulagin, et al., "Theoretical and experimental studies of relativistic oversized Ka-band surface-wave oscillator based on 2D periodical corrugated structure", *Phys. Rev. Accel. and Beams*, vol. 21, no. 080701, Aug. 2018, doi: 10.1103/PhysRevAccelBeams.21.080701

[8] A. M. Malkin, I. V. Zheleznov, A. S. Sergeev, and N. S. Ginzburg, "Quasi-optical theory of relativistic Cherenkov surface-wave oscillators with oversized cylindrical waveguides", *Phys. Plasmas*, vol. 28, no. 063102, June 2021, doi:10.1063/5.0047087

[9] A. M. Malkin, A. E. Fedotov , V. Yu. Zaslavsky , S. E. Fil'chenkov, A. S. Sergeev, E. D. Egorova , and N. S. Ginzburg, "Relativistic Sub-THz Surface-Wave Oscillators With Transverse Gaussian-Like Radiation Output" vol. 42, no.5, pp.751-754, May 2021, *IEEE. Electron. Dev. Lett*., doi: 10.1109/LED.2021.3067170; A. M. Malkin , N. S. Ginzburg, V. Zaslavsky, I. V. Zheleznov and A. S. Sergeev, "Quasi-Optical Theory of Relativistic Cherenkov Oscillators and Amplifiers with Oversized Electrodynamic Structures", *MDPI Electronics*, vol. 11, no. 1197. Apr. 2022, doi:10.3390/electronics11081197

[10] I. V. Konoplev, L. Fisher, A. W. Cross, A. D. R. Phelps, K. Ronald, M. Thumm, "Excitation of surface field cavity and coherence of electromagnetic field scattering on two-dimensional cylindrical lattice", *Appl. Phys. Lett*., vol. 97, no. 261102, Dec. 2010, doi: 10.1063/1.3529953

[11] A. J. MacLachlan, C. W. Robertson, A. W. Cross and A. D. R. Phelps, "Efficient, 0.35 THz Overmoded Oscillator Based on a Two-Dimensional Periodic Surface Lattice", *IEEE Trans. Electron Dev.*, vol.69, no.11, pp. 6342-6347, Nov. 2022, 10.1109/TED.2022.3209142

[12] D. K. Abe, Y. Carmel, S. M. Miller, A. Bromborsky, B. Levush, T. M. Antonsen, Jr., and W. W. Destler, "Experimental studies of overmoded relativistic backward-wave oscillators," *IEEE Trans. Plasma Sci*., vol. 26, no. 3, pp. 591-604, June 1998, doi: 10.1109/27.700796

[13] A. N. Vlasov, A. G. Shkvarunets, J. C. Rodgers, Y. Carmel, T. M. Antonsen, T. M. Abuelfadl, D. Lingze, V. A. Cherepenin, G. S. Nusinovich, M. Botton and V. L. Granatstein, "Overmoded GW-class surface-wave microwave oscillator," *IEEE Trans. Plasma Sci*., vol. 28, no. 3, pp. 550–560, June 2000, doi: 10.1109/27.887671

[14] G. Wang, J. Wang, P. Zeng, D. Wang, and S. Li, "Mode competition and selection in overmoded surface wave oscillator", *Phys. Plasmas*, vol. 23, no. 053113, May 2016 doi: 10.1063/1.4951021

[15] J. Wang, G. Wang, D. Wang, S. Li, P. Zeng, "Megawatt-level surface wave oscillator in Y-band with large oversized structure driven by annular relativistic electron beam", *Nature Scientific Reports*, vol.8, No. 6978, May 2018, doi:10.1038/s41598-018-25466-w

[16] Y. Annaka , K. Ogura , K. Rachi, Y. Hoshi, S. Kubo , T. Shimozuma, S. Kobayashi, and K. Okada, "Design and Fabrication of 200-GHz Oversized Surface-Wave Oscillator", *IEEE Trans. Plasma Sci*., vol.49, pp. 33-39, June 2020, doi:10.1109/TPS.2020.2998119

[17] H. A. Hafez, X. Chai, A. Ibrahim, S. Mondal, D. Férachou, X. Ropagnol and T. Ozaki, "Intense terahertz radiation and their applications," *J. Opt.*, vol. 18, no. 9, Aug. 2016. doi: 10.1088/2040-8978/18/9/093004

[18] E. A. Nanni, A. B. Barnes, R. G. Griffin and R. J. Temkin, "THz dynamic nuclear polarization NMR", *IEEE Trans. THz Sci. Technol.*, vol. 1, no. 1, pp. 145-163, Sept. 2011, doi: 10.1109/TTHZ.2011.2159546

[19] J. Federici and L. Moeller, "Review of terahertz and subterahertz wireless communications," *J. Appl. Phys*., vol. 107, no. 111101, June 2010, doi: 10.1063/1.3386413

[20] A. Dobroiu, M. Yamashita, Y. N. Ohshima, Y. Morita, C. Otani, and K. Kawase, "Terahertz imaging system based on a backward-wave oscillator," *Appl. Opt.*, vol. 43, no. 30, pp. 5637–5646, Oct. 2004, doi: 10.1364/ao.43.005637

[21] A. Feintuch et al., "A Dynamic Nuclear Polarization spectrometer at 95 GHz/144 MHz with EPR and NMR excitation and detection capabilities", *J. Magn. Reson.*, vol. 209, no. 2, pp. 136-141, Apr. 2011.

[22] Yu. A. Grishin, M. R. Fuchs, A. Schnegg, A. A. Dubinskii, B. S. Dumesh, F. S. Rusin, V. L. Bratman, and K. Möbius, "Pulsed Orotron - A new microwave source for submillimeter pulse high-field electron paramagnetic resonance spectroscopy", *Rev. Sci. Instrum*. vol. 75, no. 2926, June, 2004, doi: 10.1063/1.1778071

[23] G. Doucas, V. Blackmore, B. Ottewell, C. Perry, P. G. Huggard, E. Castro-Camus, M. B. Johnston, J. Lloyd Hughes, M. F. Kimmitt, B. Redlich, and A. van der Mee, "Longitudinal electron bunch profile diagnostics at 45 MeV using coherent Smith-Purcell radiation", *Phys. Rev. ST Accel. Beams*, vol.9, no. 092801, Sept. 2006, doi:10.1103/PhysRevSTAB.9.092801

[24] J. Feng, Y. Tang, D. Gamzina, X. Li, M. Gonzalez, R. Barchfeld, H. Li, P. Pan, R. Letizia, C. Paoloni, N. C. Luhmann Jr., "Fabrication of a 0.346-THz BWO for Plasma Diagnostics", *IEEE Trans. Electron. Dev.* vol. 65, no. 6, pp.2156-2163, June 2018, doi: 10.1109/TED.2018.2821683

[25] M. A. K. Othman, M. Veysi, A. Figotin, and F. Capolino, "Giant amplification in degenerate band edge slow-wave structures interacting with an electron beam", *Phys. Plasmas*, vol.23, no. 033112, Mar. 2016, doi: 10.1063/1.4942791

[26] M. A. K. Othman, V. A. Tamma, and F. Capolino, "Theory and New Amplification Regime in Periodic Multimodal Slow Wave Structures With Degeneracy Interacting With an Electron Beam", *IEEE. Trans. Plasma Sci*. vol. 44, no.4, pp.594-611, Apr. 2016, doi:10.1109/TPS.2016.2538786

[27] A. F. Abdelshafy, M. A. K. Othman, F. Yazdi, M. Veysi, A. Figotin, and F. Capolino, "Electron-Beam-Driven Devices With Synchronous Multiple Degenerate Eigenmodes", *IEEE. Trans. Plasma Sci*. vol. 46, no.8, pp.3126-3138, Aug. 2018, doi: 10.1109/TPS.2018.2852733

[28] A. F. Abdelshafy, D. Oshmarin, M. A. K. Othman, M. M. Green and F. Capolino, "Distributed Degenerate Band Edge Oscillator" *IEEE. Trans. Antennas Propag.*, vol. 69, no.3, pp. 1821-1824, Mar. 2021, doi: 10.1109/TAP.2020.3018539.

[29] A. J. MacLachlan, C. W. Robertson, I. V. Konoplev, A. W. Cross, A. D. R. Phelps and K. Ronald, "Resonant excitation of volume and surface fields on complex electrodynamic surfaces", *Phys. Rev. Appl*., vol. 11, no. 034034, Mar. 2019, doi: 10.1103/PhysRevApplied.11.034034

[30] A. J. MacLachlan, C. W. Robertson, K. Ronald, A. W. Cross and A. D. R. Phelps, "Mode coupling in periodic surface lattice and metamaterial structures for mm-wave and THz applications", *SN Appl. Sciences*, vol. 1, no. 613, May 2019, doi: 10.1007/s42452-019-0596-z

[31] A. J. MacLachlan, C. W. Robertson, A. W. Cross, K. Ronald and A. D. R. Phelps, "Excitation and coupling of volume and surface fields on complex electrodynamic surfaces at mm-wave and THz frequencies", *IET Microw. Antennas Propag.,* vol. 14, pp.1151-1156, May 2020, doi:10.1049/iet-map.2019.1165

[32] M. Garven, S. N. Spark, A. W. Cross, S. J. Cooke, and A. D. R. Phelps, "Gyrotron Experiments Employing a Field Emission Array Cathode", *Phys. Rev. Lett*, vol. 77, no. 11, Sept. 1996, doi:10.1103/PhysRevLett.77.2320

[33] P. MacInnes, C. R. Donaldson, C. G. Whyte, A. J. MacLachlan, K. Ronald, A. D. R. Phelps, and A. W. Cross, " Numerical analysis of high-power X-band sources, at low magnetic confinement, for use in a multi-source array". *IEEE Trans. Electron Dev.*, vol. 69*,* no.(1), pp. 340-346, Jan. 2022, doi:10.1109/TED.2021.3130503

[34] A. Vlasov, G. Nusinovich, B. Levush A. Bromborsky, W. Lou, and Y. Carmel, "Relativistic backward-wave oscillators operating near cyclotron resonance", *Phys. of Fluids B: Plasma Phys.,* vol. 5, no. 1625, pp.1625-1638, Feb. 1993, doi: /10.1063/1.860902

[35] Y. Choyal, K. Minami, and V. L. Granatstein, "Slow Cyclotron Instability in a High-Power Backward-Wave Oscillator", *IEEE Trans. Plasma. Sci*., vol. 32, no.6, pp.2157-2168, Dec. 2004, doi: 10.1109/TPS.2004.835972

[36] I. V. Bandurkin and A. V. Savilov, "Super-radiant Cherenkov backward-wave oscillator with cyclotron absorption", *Appl. Phys. Lett*., vol. 99, no. 193506, Nov. 2011, doi:10.1063/1.3659693

[37] A. J. MacLachlan, C. W. Robertson, A. W. Cross, and A. D. R. Phelps, "Data underpinning this publication is available from the University of Strathclyde KnowledgeBase at,"Univ. Strathclyde, Glasgow, U.K., Tech. Rep., 2022, doi: 10.15129/7955dd51-b38d-4119-9ce7- b1592e502f0d